

Theoretical demonstration of highly efficient cw THz generation by using composite photonic-structure elements

A. Oyamada

a-oyamada@pe.osakafu-u.ac.jp

H. Kitaguchi

K. Ebata

H. Ishihara

Department of Physics and Electronics, Osaka Prefecture University 1-1 Gekuen-cho, Naka-ku, Sakai, Osaka 599-8531, Japan

Department of Physics and Electronics, Osaka Prefecture University 1-1 Gekuen-cho, Naka-ku, Sakai, Osaka 599-8531, Japan

Industrial Materials and Process Technology R&D Laboratories, Sumitomo Electric Industries, Ltd.1-1-1, Koyakita, Itami-shi, Hyogo 664-0016, Japan

Department of Physics and Electronics, Osaka Prefecture University 1-1 Gekuen-cho, Naka-ku, Sakai, Osaka 599-8531, Japan

We theoretically propose one-dimensional composite photonic structures for high-resolution THz spectroanalysis. We compare the performance of two GaAs/AlAs composite photonic-structure devices, one with usual 1/4-wavelength layers of distributed Bragg reflectors (DBRs), and the other with the designed DBRs. The device with designed DBRs shows the optical-to-terahertz conversion efficiency up to 10^{-5} and wide frequency tunability ranging from sub-THz to 3 THz. We found that the composite photonic structure allows us to control photonic modes with a high degree of freedom by flexible structure designs. This device achieve a cw THz source with a highly narrow bandwidth operating at room temperature.

[DOI: <http://dx.doi.org/10.2971/jeos.2013.13023>]

Keywords: THz generation, one-dimensional photonic crystal, difference frequency generation

1 INTRODUCTION

Recently, high-resolution THz spectroanalysis using THz comb is reported [1]. Although the THz comb is a powerful technique for high-resolution THz spectroanalysis, this technique needs two mode-lock lasers. In order to analyze spectroscopy with low cost and compact system, we need tunable continuous wave (cw) THz source that can generate THz wave of wide frequency range. Especially around 1THz, quantum cascade lasers [2], photomixing technique [3], and back wave oscillators (BWO) [4] are known as plausible cw terahertz sources. However, until now, quantum cascade laser has difficulty in tunability, output of the photomixing technique is low over 1 THz, and the BWO requires extra-high voltage to be operated. In the present work, we focus on difference frequency generation (DFG) process in photonic structures. By utilizing photonic band-edge (PBE) modes, one can obtain intensive nonlinear optical effect such as wavelength conversion [5, 6]. A Wavelength-conversion laser by photonic structures is greatly suited for the narrow line-width wave source and can be operated at room temperature. Then, THz generation with photonic structures have attracted much attentions [7]–[9].

Here, we consider one-dimensional composite photonic structures that consist of two periodic photonic structures. One is the Distributed Bragg reflector (DBR) in which incident wavelength lies in photonic band gap [10], and the other is the PBE structure in which photonic band-edge effect works on the incident wave. The basic scheme for the present terahertz emis-

sion device is shown in Figure 1. Here, we use the fact that the band-edge modes for s-polarized and p-polarized waves generally have different frequencies (ω_p, ω_s) when we inject light obliquely to the crystal surface. When we tune the pump and signal frequencies ($\omega_{pump} = \omega_p, \omega_{signal} = \omega_s$) to these frequencies, respectively, THz wave is generated through difference frequency generation (DFG) ($\omega_{idler} = \omega_{pump} - \omega_{signal}$).

In this paper, we compare two types of composite photonic structures (Figure 2(a),(b)). One is a PBE structure sandwiched by two DBRs that consists of 1/4-wavelength layers and the other is one sandwiched by newly designed DBRs. By changing thickness of each layer in DBRs, we can control PBE modes with high degree of freedom and then can obtain strong THz wave.

2 THEORY AND MODEL

In this section, we describe how we calculate the transmission spectrum and internal field intensity for periodic multilayers. By imposing Maxwell boundary conditions at each interface, we can obtain electric fields in each layer within the linear responses ($\mathbf{E}_p, \mathbf{E}_s$). In order to derive the idler wave, we utilize the pump signal idler coupled-wave equation [11];

$$\nabla \times \nabla \times \mathbf{E}_i - \frac{\omega_i^2}{c^2} \epsilon_i \mathbf{E}_i = 2 \frac{\omega_i^2}{c^2} \mathbf{d}^{(2)} \mathbf{E}_p \mathbf{E}_s, \quad (1)$$

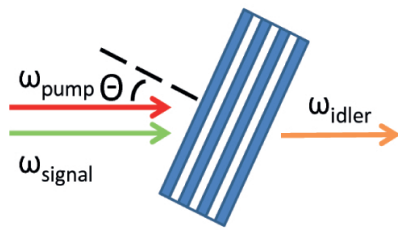


FIG. 1 Basic scheme of THz generation with a one-dimensional photonic structure.

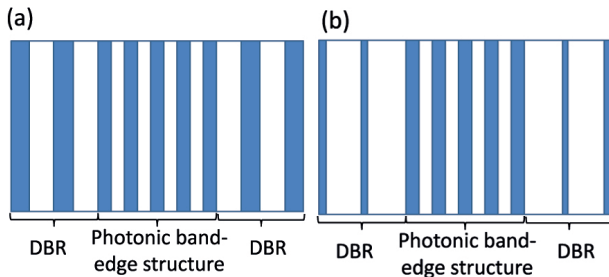


FIG. 2 (a) Composite photonic structure with 1/4-wavelength DBRs (structure A). (b) Composite photonic structure with designed DBRs (structure B).

where E_p , E_s , E_i are pump, signal, and idler electric fields, respectively. $\mathbf{d}^{(2)}$ is the second nonlinear coefficient tensor. ω_i and c are the idler angular frequency and the velocity of light in vacuum. We obtain the particular solution of the Eq. (1) with Green's function method as

$$E_i = 2 \frac{\omega_i^2}{c^2} \int \mathbf{G}(\mathbf{r}; \mathbf{r}') \mathbf{d}^{(2)} E_p E_s d\mathbf{r}. \quad (2)$$

$\mathbf{G}(\mathbf{r}; \mathbf{r}')$ is dyadic Green's function [12] as

$$\mathbf{G}(\mathbf{r}; \mathbf{r}') = \frac{i}{8\pi^2} \int \int_{\infty} d\mathbf{k}_s e^{i\mathbf{k}_s(\mathbf{r}_s - \mathbf{r}'_s) + ik_{0z}|z - z'|} \times \left[\frac{\mathbf{I}k_0^2 - \mathbf{k}_0\mathbf{k}_0}{k_0^2 k_{0z}} \right] - \frac{\hat{z}\hat{z}}{k_0^2} \delta(\mathbf{r} - \mathbf{r}'), \quad (3)$$

where, \mathbf{k}_s and \mathbf{r}_s are the wave vector and the position vector parallel to the interfaces, and k_{0z} is wave vector component vertical to the interfaces. Wave vector in the media is given by $\mathbf{k}_0 = \mathbf{k}_s + \hat{z} \text{sgn}(z - z') k_{0z}$, and k_0 is $|\mathbf{k}_0|$. Because Eq. (3) is the expression used for free space, we should impose Maxwell boundary conditions on E_i at each layer.

We consider GaAs/AlAs multilayers. Here, we assume that the second nonlinear tensor components for GaAs layers are $d_{14} = d_{25} = d_{36} = 90.1 \text{ pm/V}$ [13] and ignore those for AlAs. We also assume that the structures are grown on (110) surface. As for intensities of pump and signal wave, both of them are focused sufficiently to be 1 MW/cm^2 that is below the damage threshold of the sample for the operating frequency. In this paper, we make a comparison of two composite photonic structures. One is the composite photonic structure with 1/4-wavelength DBRs (Structure A). The number of multilayer period of the PBE structure for Structure A is 12.5 and that of each DBR is 14. We assume that the PBE structure consists of 72.5 nm-thick GaAs and 84.7 nm-thick AlAs, and the DBR consists of 79.2 nm-thick GaAs and 92.5 nm-thick AlAs. Total size of Structure A is $6.8 \text{ }\mu\text{m}$. The other is the composite photonic structure with designed DBR (Structure B). The number of multilayer period of the PBE structure for Structure B is 44.5

and that of each DBR is 30. We assume that the PBE structure consists of 74.5-nm-thick GaAs and 87-nm-thick AlAs, and the DBR consists of 31-nm-thick GaAs and 145-nm-thick AlAs. Total size of Structure B is $17.8 \text{ }\mu\text{m}$. For these structures, we determine that the minimum values of the full width at half maximum (FWHM) for both s- and p-polarized transmission modes are equal to 0.01 nm (2.7 GHz).

3 RESULTS

Figures 3(a)–(d) show the transmission spectrum of Structure A and B when the incident angle is set to be 60. When we inject waves obliquely, PBE mode usually shifts toward short wavelength. Here, we assume that the p-polarized transmission resonant mode is kept on 1064 nm by controlling temperature of the samples (Figure 3(e)) [14]. The FWHM of the p-polarized mode of Structure A becomes large (Figure 3(b)). This fact implies the low Quality factor (Q-factor) of this mode. In contrast, the FWHM of the s-polarized mode become small. This is due to the different transmissions at interfaces for different polarized beams. For the Structure A, Q-factor of the s-polarized mode increases as incident angle increases, whereas that of the p-polarized mode decreases. Thus, the Structure A cannot achieve high Q-factor for both s- and p-polarized fields simultaneously, and consequently, the conversion efficiency is limited by this mechanism. In order to overcome this problem, we consider the Structure B with the designed DBR. This DBR mirror acts as high reflectivity mirror for p-polarized band-edge mode, and at the same time, acts as low reflectivity mirror for s-polarized band-edge mode. By using Structure B we can suppress the increase of FWHM for the p-polarized mode (Figure 3(d)) and can achieve high Q-factor for both modes. The angle dependencies of Q-factor of these two modes are shown in Figure 3(f). The Structure B enhances s- and p-polarized fields simultaneously and we can realize much higher conversion efficiency.

We normalized the intensities of internal fields with the incident intensity and show them as functions of position in Figure 4(a),(b). The normalized internal intensity of p-polarized wave for the Structure A is lower than that for the Structure B, which can be explained by the Q-factors in Figure 3(f). In the same way, the normalized internal intensity of the s-polarized wave is higher than that of p-polarized one in both Structures. As for s-polarized wave, an optical enhancement effect of Structure A appears to be higher than that of Structure B. However, the Q-factor of Structure B becomes higher because of difference of the total crystal lengths. Consequently, the optical enhancement effect of the s- and p-polarized waves of Structure B is stronger than that of Structure A and the former achieves higher conversion efficiency ($\eta = P_{\text{THz}} / (P_{\text{pump}} + P_{\text{signal}})$) (Figure 4(c)). Here, it should be remarked that we need not consider phase matching condition because the crystal lengths (order of $10 \text{ }\mu\text{m}$) are much shorter than the coherent length (order of $100 \text{ }\mu\text{m}$), so that the conversion efficiencies increase in proportion to the square of the crystal lengths. The output frequency of two Structures is shown as a function of incident angle in Figure 4(d). Output frequency is equal to the frequency difference of the two modes, i.e. the p-polarized mode and the s-polarized mode.

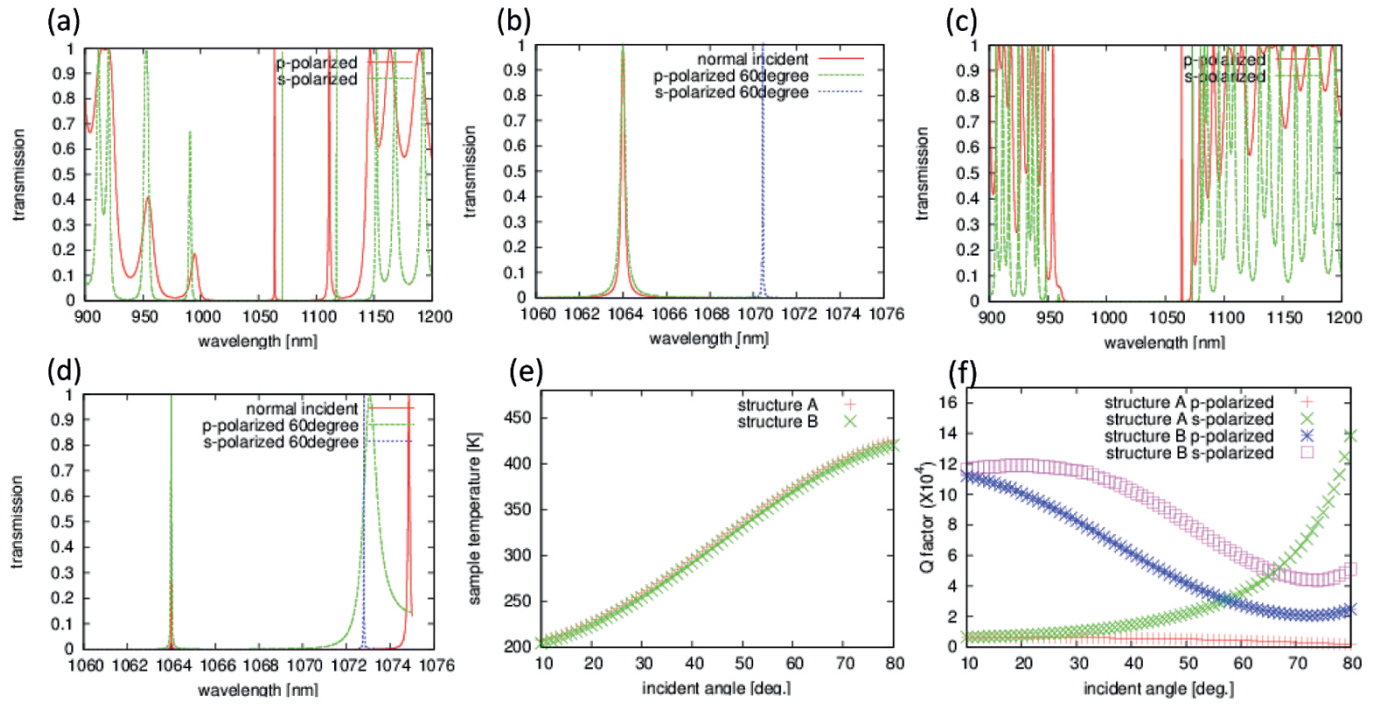


FIG. 3 Transmission spectra of 60 degree incident and angle dependence of sample temperature and of quality factor. (a) Transmission spectrum of 60 degree incident for Structure A with wide frequency range. (b) Transmission spectrum of normal or 60 degree incident for Structure A with narrow frequency range. (c) Transmission spectrum of 60 degree incident for Structure B with wide frequency range. (d) Transmission spectrum of normal or 60 degree incident for Structure B with narrow frequency range. (e) Angle dependence of sample temperature for Structure A,B. (f) Angle dependence of quality factor for Structure A,B.

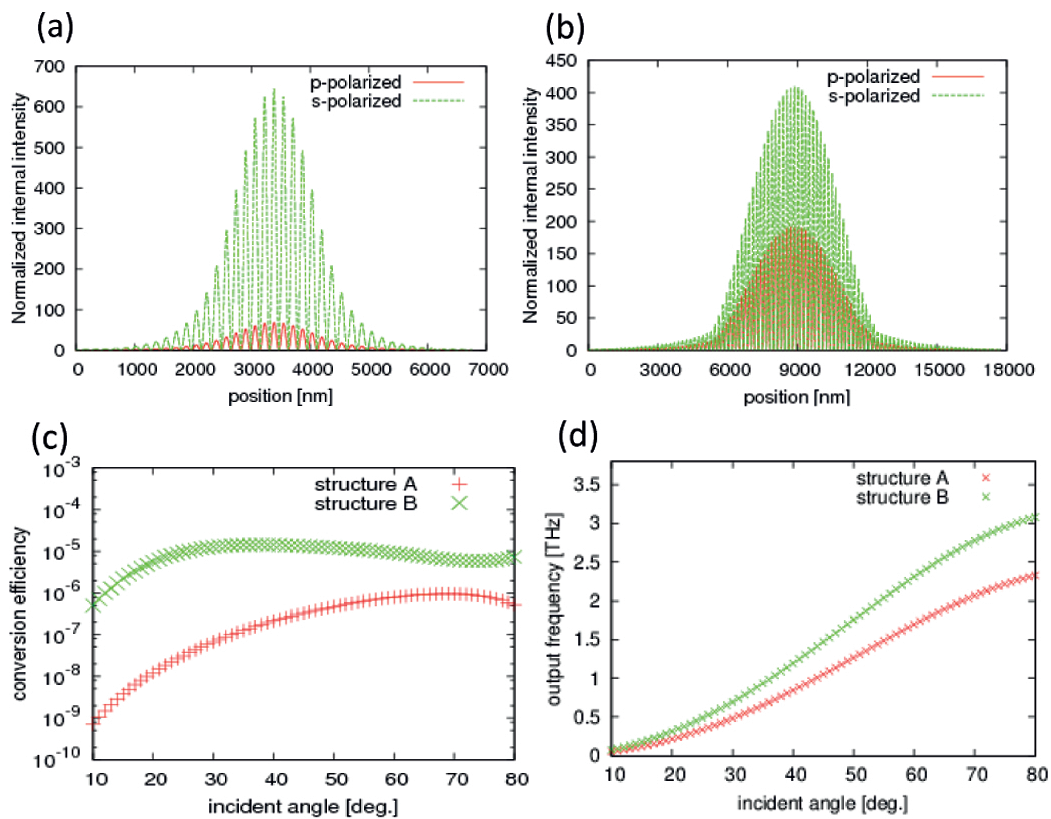


FIG. 4 Field intensities of 60 degree incident normalized with incident intensity in the Structure A,B and angle dependencies of conversion efficiency and of frequency. (a) Intensity profile in the Structure A. (b) Intensity profile in the Structure B. (c) Angle dependencies of conversion efficiency for the structures. (d) Angle dependencies of output frequency for the structures.

As incident angle increases, output frequency becomes larger. In other words, output frequency can be tuned by incident angle. Structure A can generate waves with the frequency rang-

ing from 0 to 2.3 THz and Structure B can cover from 0 to 3.0 THz. The difference of covering range arises from the number of period of photonic structure. The more layers photonic

structure has, the wider THz frequency range we can generate.

4 CONCLUSION

Composite photonic structure allows us to control photonic modes with a high degree of freedom by flexible structure design utilizing two kinds of periodic patterns. We theoretically demonstrated that the flexibility enables us to achieve high performance cw THz source with an optical-to-THz conversion efficiency up to 10^{-5} and a frequency tunability ranging from sub-THz to 3 THz. The bandwidth of THz wave is expected to have the same level as that of the incident beam due to the parametric process. Therefore, when we use narrow bandwidth tunable lasers as pump and signal waves, we can generate narrow bandwidth THz wave. Furthermore, because DFG process can be operated at room temperature, we can provide versatile THz source for high-resolution THz spectro-analysis. Experimental demonstration is desired in order to exploit full potential of this device in the future.

5 ACKNOWLEDGEMENTS

The authors are grateful to T. Shimomura in Ehime University and Y. Shim in Osaka Prefecture University for valuable discussions. They also thanks H. Horinaka and K. Wada in Osaka Prefecture University for helpful advices.

References

- [1] T. Yasui, Y. Kabetani, E. Saneyoshi, S. Yokoyama, and T. Araki, "Terahertz frequency comb by multifrequency-heterodyning photoconductive detection for high-accuracy, high-resolution terahertz spectroscopy," *Appl. Phys. Lett.* **88**, 241104 (2006).
- [2] C. Walther, M. Fischer, G. Scalari, R. Terazzi, N. Hoyler, and J. Faist, "Quantum cascade lasers operating from 1.2 to 1.6 THz," *Appl. Phys. Lett.* **91**, 131122 (2007).
- [3] F. Hindle, A. Cuisset, R. Bocquet, and G. Mouret, "Continuous-wave terahertz by photomixing: applications to gas phase pollutant detection and quantification," *C. R. Physique* **9**, 262-275 (2008).
- [4] G. P. Gallerano, and S. Biedron, "Overview of terahertz radiation sources," in *Proceedings of the 2004 FEL Conference*, 216-221 (Sincrotrone Trieste S.C.p.A, Trieste, 2004).
- [5] G. D. Aguanno, M. Centini, M. Scalora, C. Sibilia, M. J. Bloemer, C. M. Bowden, J. W. Haus, and M. Bertolotti, "Group velocity, energy velocity, and superluminal propagation in finite photonic band-gap structures," *Phys. Rev. E* **63**, 036610 (2001).
- [6] H. Yang, P. Xie, S. K. Chan, Z. Q. Zhang, I. K. Sou, G. K. L. Wong, and K. S. Wong, "Efficient second harmonic generation from large band gap II-VI semiconductor photonic crystal," *Appl. Phys. Lett.* **87**, 131106 (2005).
- [7] T. Kitada, F. Tanaka, T. Takahashi, K. Morita, and T. Isu, "GaAs/AlAs coupled multilayer cavity structures for terahertz emission devices," *Appl. Phys. Lett.* **95**, 111106 (2009).
- [8] K. Saito, T. Tanabe, and Y. Oyama, "THz-Wave Generation from GaP THz Photonic Crystal Waveguides under Difference-Frequency Mixing," *OPJ* **2**, 201-205 (2012).
- [9] T. Chen, J. Sun, L. Li, J. Tang, and Y. Zhou, "Design of a Photonic Crystal Waveguide for Terahertz-Wave Difference-Frequency Generation," *IEEE Photonic. Tech. L.* **24**, 921-923 (2012).
- [10] E. Yablonovitch, "Photonic band-gap structures," *JOSA B* **10**, 283-295 (1993).
- [11] R. W. Boyd, *Nonlinear Optics* (Third Edition, Academic Press, San Diego, 2008).
- [12] W. C. Chew, *Waves and Field in Inhomogeneous Media* (IEEE Press, New York, 1995).
- [13] B. F. Levine, and C. G. Bethea, "Nonlinear Susceptibility of GaP; Relative Measurement and Use of Measured Values to Determine a Better Absolute Value," *Appl. Phys. Lett.* **20**, 272 (1972).
- [14] J. Talghader, and J. S. Smith, "Thermal dependence of the refractive index of GaAs and AlAs measured using semiconductor multilayer optical cavities," *Appl. Phys. Lett.* **66**, 335 (1995).